tvst

DOI: 10.1167/tvst.3.3.5

Article

A Test of a Model of Glaucomatous Damage of the Macula With High-Density Perimetry: Implications for the Locations of Visual Field Test Points

Donald C. Hood[1,2], Matthew Nguyen[1], Alyssa C. Ehrlich[1], Ali S. Raza[1,3], Ieva Sliesoraityte[4,5], Carlos G. De Moraes[2], Robert Ritch[6,7], and Ulrich Schiefer[4,8]

[1] Department of Psychology, Columbia University, New York, NY
[2] Department of Ophthalmology, Columbia University, New York, NY
[3] Department of Neurobiology and Behavior, Columbia University, New York, NY
[4] Centre for Ophthalmology, University of Tübingen, Tübingen, Germany
[5] Institut de la Vision, INSERM CIC 503, Paris, France
[6] Einhorn Clinical Research Center, New York Eye and Ear Infirmary, New York, NY
[7] Department of Ophthalmology, New York Medical College, Valhalla, NY
[8] Competence Centre "Vision Research", University of Applied Sciences, Aalen, Germany

Correspondence: Donald C. Hood, Department of Psychology, 406 Schermerhorn Hall, 1190 Amsterdam Avenue, MC 5501, Columbia University, New York, NY 10027; dch3@columbia.edu

Received: 22 March 2014
Accepted: 28 April 2014
Published: 19 June 2014

Keywords: glaucoma; macula; visual fields; perimetry; test point location

Citation: Hood DC, Nguyen M, Ehrlich AC, et al. A test of a model of glaucomatous damage of the macula with high-density perimetry: implications for the locations of visual field test points. Tran Vis Sci Tech. 2014;3(3):5, http://tvstjournal.org/doi/full/10.1167/tvst.3.3.5, doi: 10.1167/tvst.3.3.5

Purpose: To use high-density perimetry to test a model of local glaucomatous damage to the macula (central visual field [VF]) and to assess the optimal placement of stimuli used to detect this damage.

Methods: Thirty-one eyes of 31 patients showing glaucomatous arcuate damage within the upper hemifield of the central 10° were tested with a customized VF with double the density of the 10-2 (2° grid) test. Individual plots of total deviation (TD) values were generated. A model, which predicts a "vulnerable macular region" (VMR) and a "less vulnerable macular region" (LVMR), was compared with the TD values without (standard model) and with (aligned model) scaling and rotating to align it with the patient's fovea-to-disc axis. Computer simulations assessed alternative VF locations for adding two points to the 6° grid pattern (e.g., 24-2 VF) typically used in the clinic.

Results: There were significantly more abnormal points in the VMR than in the LVMR. However, the aligned model did no better than the standard model in describing the data. The optimal locations for adding two points to the 24-2 (6° grid) test were (−1°, 5°) and (1°, 5°), both within the VMR.

Conclusions: The model describes the region of the superior VF vulnerable to arcuate damage.

Translational Relevance: The model can be used to determine the optimal locations for adding test points to the commonly used VF test pattern (24-2). It does not seem necessary to adjust the location of VF test points based upon interindividual differences in the fovea-to-disc axis.

Introduction

The macula, defined here as the central ±8°, contains over 30% of the total retinal ganglion cells (RGCs),[1] and is the most important region of the retina for many essential day-to-day visual functions such as driving and reading.[2,3] Recent combined visual field (VF) and optical coherence tomography (OCT) data provide unequivocal evidence that glaucoma affects this region even in the early/initial stages of the disease.[4–6] This work is consistent with earlier VF studies illustrating glaucomatous damage of the macula.[7–17] While macular damage may have a relatively mild diffuse component,[6] of particular concern are the deep localized defects close to fixation, which occur largely in the upper VF.[5,13–15,18]

To better understand these defects, we[18] previously

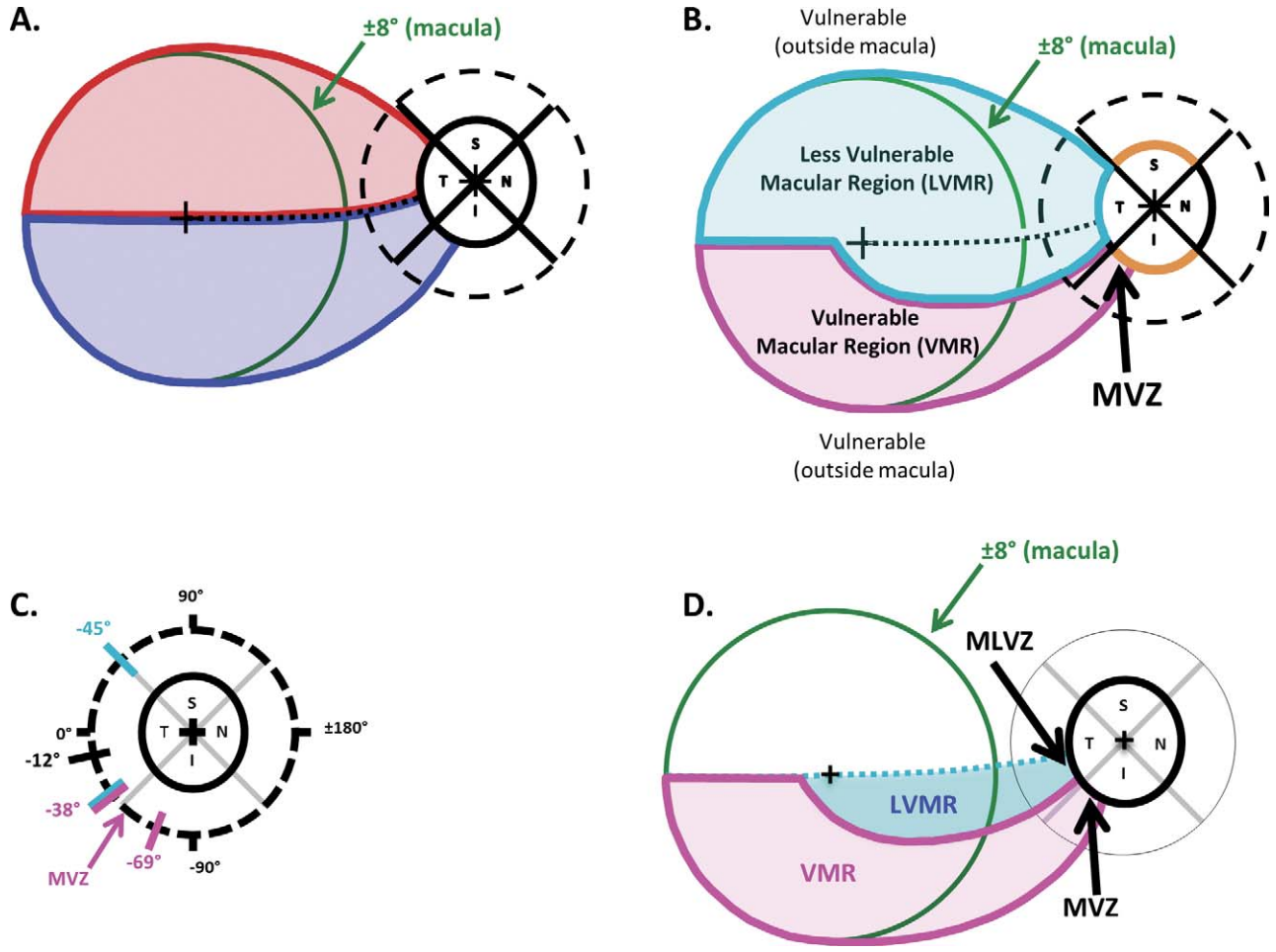

Figure 1. (A) According to a recent model,[4–6] on average the axons from the RGCs in the superior and inferior macular regions (i.e., within the ±8° *green circle*) fall within the *red* and *blue* regions, respectively. The RGC axons in the superior region of the macula enter the optic disc in the temporal quadrant (*red*), while those in the lower macula enter in the inferior, as well as the temporal quadrant (*blue*). (B) According to the model, there is a VMR (*magenta*) and a LVMR (*cyan*). The VMR is associated with the MVZ of the disc. (C) The regions of the disc associated with the VMR and LVMR are indicated by the *magenta* and *cyan diagonal lines*, respectively. (D) The portion of the model in *panel B* associated with the upper visual field (inferior retina) is shown; it contains a LVMR (*cyan*) and a VMR (*magenta*).

studied 11 eyes with arcuate-like defects on the 10-2 VF test, but without defects outside the central 10° on the 24-2 VF (6° grid) test. In 10 of 11 eyes, the defect was in the upper VF. On circumpapillary OCT circle scans of the optic disc, the point of maximum thinning of the retinal nerve fiber layer (RNFL) fell in a very narrow region for all 10 eyes. This region, subsequently called the macular vulnerability zone (MVZ),[4,5] is largely in the inferior quadrant of the disc.

To help understand the nature of macular damage, we recently proposed a model.[4-6] The thin green circles in Figures 1A, 1B, and 1D have a radius of 8° and represent the outer border of the macula. The centers of the fovea and disc are indicated by the + symbols. The model has two main assumptions. First, anatomically it assumes that, on average, there is an asymmetric pattern of projections from the RGCs to the optic disc as shown in Figure 1A. In particular, the RGCs in the superior portion of the macula, within the red borders of Figure 1A, project to the temporal quadrant of the disc, while the RGCs in the inferior region of the macula, within blue borders, project to both the temporal and inferior quadrants. Second, the model, in agreement with previous findings,[5] assumes that the probability of local, arcuate RNFL defects is highest in and near the superior and inferior quadrants of the disc (orange arcs in Figs. 1A, 1B). The anatomical boundaries of the model (Fig. 1C) were based largely on OCT

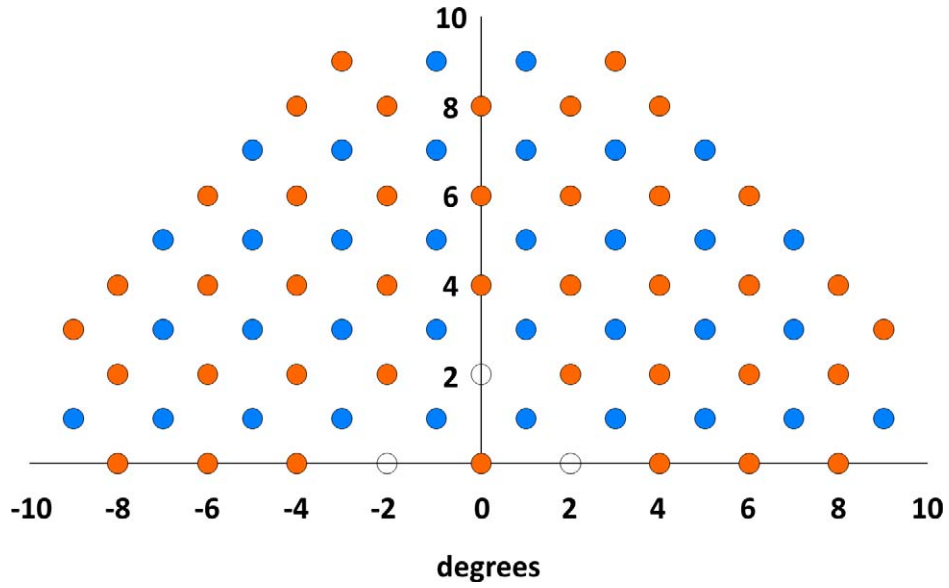

Figure 2. The locations of the high-density visual field test points. The *blue points* indicate the locations of the test points of the 2° (10-2) pattern. The *orange points* were added to create a test pattern with double the density of test points. The locations indicated by the *open symbols* were not tested because the horizontal and vertical bars of the fixation cross cover these locations.

results, including the location of the MVZ of the disc previously identified.[18]

According to the model, the superior macular region and the cecocentral portion of the inferior macula are relatively less vulnerable to macular damage; this is the region within the cyan borders of Figure 1B labeled "less vulnerable macular region" (LVMR). The regions outside of the LVMR are more vulnerable, including the inferior macular region labeled "vulnerable macular region" (VMR) and the associated region, the MVZ, near the disc.

The focus of this study is on the inferior retina (upper VF), the region shaded in Figure 1D and containing the region vulnerable to the local deep defects close to fixation. One purpose of the present study was to test the model of this region with high resolution VF data. A second purpose was to test the hypothesis that the model will better describe the VF results for individual patients if we align the fovea and disc centers by rotating and scaling the model.[17] This test speaks to a practical aspect of VF tests for glaucoma. In particular, should we take into consideration individual differences in the position of the disc relative to the fovea when designing VF tests? Finally, we illustrate how the model can be used to answer the following question: where should additional points be placed to improve the ability of the most commonly used clinical VF test (i.e., the 24-2 test pattern) to detect macular damage?

Methods

Subjects

Thirty-one eyes from 31 patients were tested. Nineteen of the patients were tested in New York City at Columbia University and 12 were tested in Tübingen, Germany at the University of Tübingen. Patients were selected by ophthalmologists according to the following criteria: all had local defects within the central 10° of the superior VF. The selection was based upon prior 10-2 VFs (Humphrey VF Analyzer; Carl Zeiss Meditec, Inc., Dublin, CA) in New York and on VF tests with the grid 30-A (Octopus 900; Haag Streit, Inc., Köniz, Switzerland) in Tübingen. In all cases, the recruiters were unaware of the predictions of the model to be tested. Participants gave informed, written consent with a protocol that followed the Declaration of Helsinki and was approved by the institutional review boards of Columbia University, New York Eye and Ear Infirmary in New York, and of the University of Tübingen in Germany.

Visual Field Testing

Subjects took a customized, upper hemifield VF test (Octopus 900; Haag-Streit, Inc., Köniz, Switzerland) with double the density (diagonal spacing of 1.4°) of the 10-2 pattern. The custom test pattern, shown in Figure 2, was created by combining the

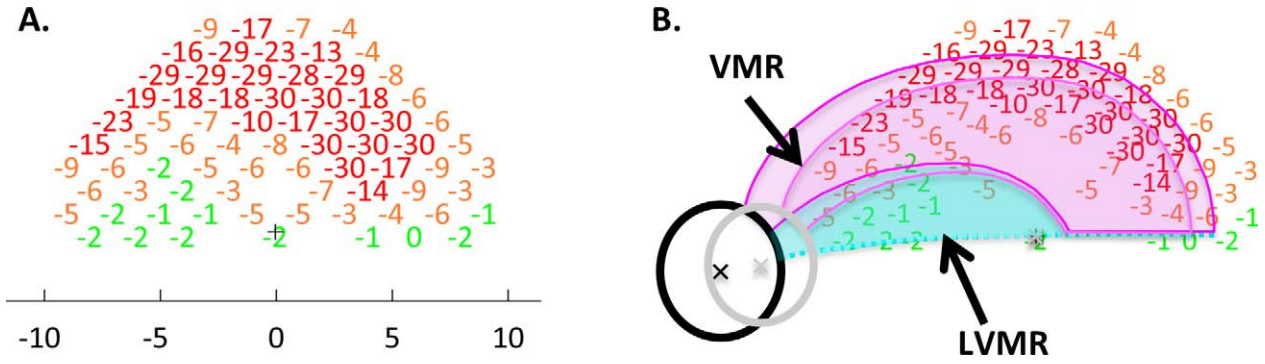

Figure 3. (A) The TD values for one of the eyes. (B) The same points are presented with the locations adjusted to account for the displacement of RGCs near the fovea.[20-22] The *black ellipse* (optic disc) and the *bold magenta* and *cyan borders* are the standard model from Figure 1D shown in field view. The *gray ellipse* and *lighter borders* represent the aligned model, formed by scaling and rotating the standard model so that its foveal and disc centers coincide with those of the patient's eye. In both panels, the TD values were color-coded as follows: *red*: ≤ -10 dB; *yellow*: ≤ -3 dB, > -10 dB; *green*: > -3 dB.

conventional 10-2 VF grid (blue points) with an additional grid of test points offset 1° up and 1° to the right (orange points). We did not test at the locations indicated by the open symbols as the horizontal and vertical bars of the fixation cross cover these locations. The test used a Goldmann stimulus size III and a fast thresholding strategy (GATE).[19] All results had reliability indices better than 30%.

Aligning the Model to Individual Eyes

First, to relate VF data to the model, the displacement of the RGCs near the fovea needed to be taken into consideration. In particular, the locations of the test points were adjusted to correspond to the location of the RGCs stimulated. This adjustment was based upon the results of postmortem human histology,[20] as previously described.[21,22] Figure 3 illustrates the adjustment of test point locations for one of the eyes in the study. In particular, Figure 3A shows the total deviation (TD) values for the 74 points of the high density VF pattern and Figure 3B, these data after adjusting the test point locations to account for RGC displacement. In both panels, the TD values were color-coded (red: ≤ -10 dB; yellow: ≤ -3 dB, > -10 dB; green: > -3 dB).

Second, the model in Figure 1D, in field view, was compared with the data in two ways. For what we call the standard model, the foveal center of the model was aligned with the central fixation point of the VF and no further adjustments were made. The result is shown as the black disc and darker lines in Figure 3B. For the aligned model, the standard model was scaled and rotated so that both the centers of the fovea and disc coincided with those of the individual eye. The result is shown as the gray disc and lighter borders. The location of the disc center relative to the foveal center was determined using en face images, either OCT shadowgrams (3D-OCT 2000; Topcon Medical Systems, Inc., Oakland, NJ) or confocal scanning laser ophthalmoscopy (Spectralis; Heidelberg Engineering, Inc., Heidelberg, Germany). To determine the location with more accuracy, the center of the fovea was marked on an OCT B-scan slice and then coregistered with the en face images.

Simulations

A custom MATLAB (version R2013a; MathWorks, Inc., Natick, MA) program was written to simulate various VF test patterns by selecting subsets of points from the high-density set of points meeting specified criteria. In particular, we chose two additional points to be added to the 24-2 test pattern so that there was the same number of points (nine) in the central 10° of the upper VF as for the G program (Haag-Streit, Inc.), which is designed to detect glaucomatous defects. To determine the optimal locations of these two additional points, the program tested all possible locations to maximize the average number of abnormal test points (TD ≤ -5 dB) across patients. The possible locations of additional points were restricted to a subset shared by the 10-2 VF test pattern. This procedure yielded more than one pair of optimal locations. The locations that most often occurred in these pairs were chosen.

Results

The Standard Model

Figure 4A shows the average TD values for the 31 eyes along with the boundaries of the standard model.

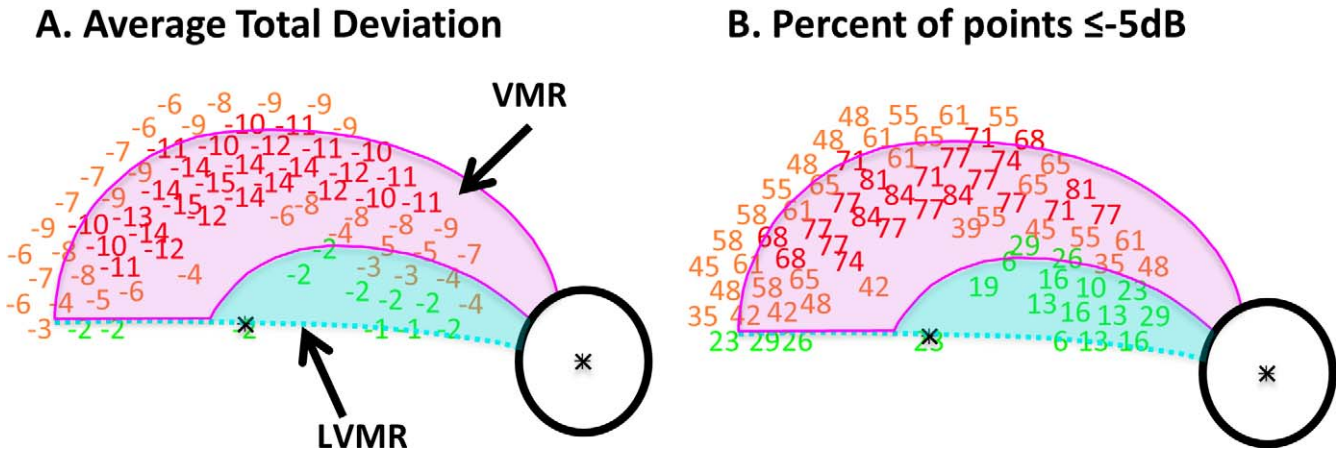

Figure 4. (A) The average TD values for the 31 eyes with the standard model as described in Figure 3. The TD values were color-coded as follows: *red*: ≤−10 dB; *yellow*: ≤−3 dB, >−10 dB; *green*: >−3 dB. (B) The average percent of points ≤−5 dB. The percentages were color-coded as follows: *red*: ≥66.7%; *yellow*: ≥33.3%, <66.7%; *green*: <33.3%.

The TD values were color-coded as in Figure 3. In agreement with the model, the deepest portion of the defect fell within the VMR of the model and this region showed a more severe VF loss than did the LVMR (i.e., the region inside the macula, but not in the VMR). In particular, the mean TD ranged from −1 to −4 dB in the LVMR and from −4 to −15 dB in the VMR. Figure 4B shows the percentage of the 31 eyes that had losses greater or equal to −5 dB at each test location of the VF; the percentages were color-coded (red: ≥66.7%; yellow: ≥33.3%, <66.7%; green: <33.3%). Notably, there is a larger percentage of abnormal VF points within the VMR as compared with the LVMR, again consistent with the standard model.

To quantitatively assess the agreement between the standard model and the data from individual eyes, the percentage of points within the VMR that were abnormal were compared with the percentage of the points within the LVMR for each eye. For this analysis, three criteria values were used to define an abnormal point: less than or equal to −10 dB, less than or equal to −5 dB, and less than or equal to −3 dB. For example, for the eye in Figure 3B, 87.8% of the points in the VMR met the less than or equal to −5 dB criteria as compared with 25.0% in the LVMR. The first row of Table 1 summarizes the results for all 31 eyes. For the standard model, the differences between the VMR and LVMR were significant at P less than 0.001 for all three criteria (Wilcoxon signed-rank test).

The Aligned Model

To assess the need for customizing the model for individual eyes, the model was fitted to an individual's data by scaling and rotating the standard model so that the centers of the fovea and disc correspond to those of the individual eye (Fig. 3). Table 1 contains the average percent of points less than or equal to −3, −5, or −10 dB in the two regions of the 31 eyes. The results were very similar for the two models. A better fit implies that the percentage of points in the VMR should be greater and the percentage of points for the LMVR should be lower for the aligned as compared with the standard model. This was only true for two of the six comparisons in Table 1. (The P values were between 0.92 and 0.29, for five of six comparisons; the sixth had too few points to qualify for the Wilcoxon signed-rank test).

As we might expect the results for the two models to be most different for the more extreme differences

Table 1. Percentage of Abnormal Points Within the VMR and LVMR for Three Criteria Values and for the Standard and Aligned Models

	Percent ≤−10 dB		Percent ≤−5 dB		Percent ≤−3 dB	
Model	VMR	LVMR	VMR	LVMR	VMR	LVMR
Standard	35.6%	3.2%	62.2%	16.4%	77.3%	34.7%
Aligned	35.3%	3.2%	61.8%	15.7%	77.2%	33.6%

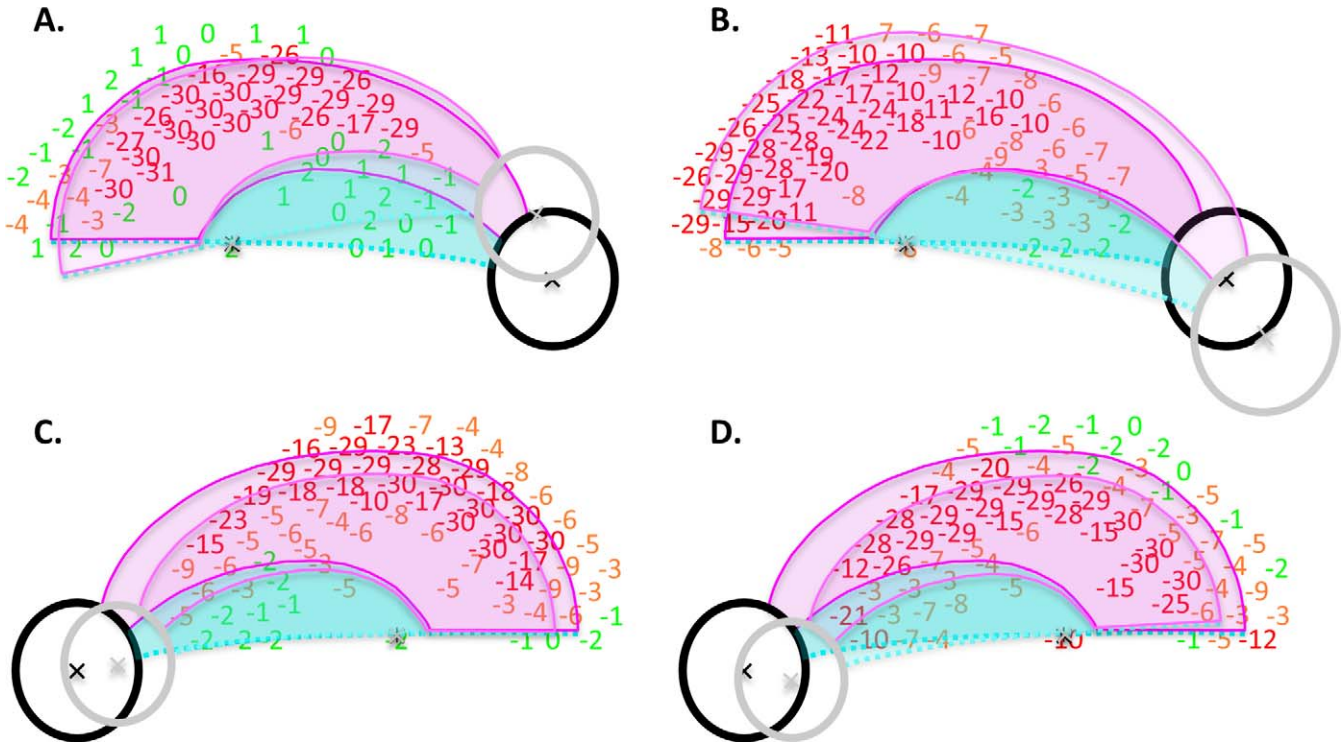

Figure 5. The TD values with the standard and aligned models displayed as in Figure 3B for two eyes (A, B) that required the most extreme rotation to account for the elevation of the disc relative to the fovea, and two eyes (C, D) that required the most extreme scaling to account for the distance between the disc and fovea.

in anatomy, Figures 5A and 5B shows two examples that required the most extreme rotation to account for the elevation of the disc relative to the fovea, and Figures 5C and 5D two that required the most extreme scaling to account for distance between the disc and fovea. In these cases, the changes were in the predicted direction for five of the eight comparisons in Table 2. While the differences were small, they do suggest a slightly better fit for the aligned model.

Adding Two Points to the 24-2 (6° Grid) Pattern

Given that the standard model does a reasonable job of describing the data for all the eyes, we can use it to simulate the outcomes for adding points to the VF. We explored the consequences of adding just two points to a standard 24-2 VF test pattern, making the total number of points the same as in the G program. Figure 6A (left panel) shows the 24-2 test points in the central 10° of the upper VF. These seven points were among the points tested by the high-density pattern in Figure 2. The right panel shows the average TD for these points from Figure 4A. The points are morphed to account for RGC displacement as in Figures 3 through 5. We simulated the 24-2 VF results for the 31 eyes tested in this study by assuming that the same thresholds would be obtained if only these seven test points were used. Table 3 contains a summary of the

Table 2. Percentage of Abnormal Points TD ≤ -5 dB Within the VMR and LVMR for the Four Eyes in Figure 5 and for the Standard and Aligned Models

	Standard Model		Aligned Model	
	VMR	LVMR	VMR	LVMR
Fig. 5A	61.0%	0.0%	67.6%	0.0%
Fig. 5B	95.1%	16.7%	96.1%	9.1%
Fig. 5C	87.8%	25.0%	84.8%	10.0%
Fig. 5D	78.0%	58.3%	88.2%	75.0%

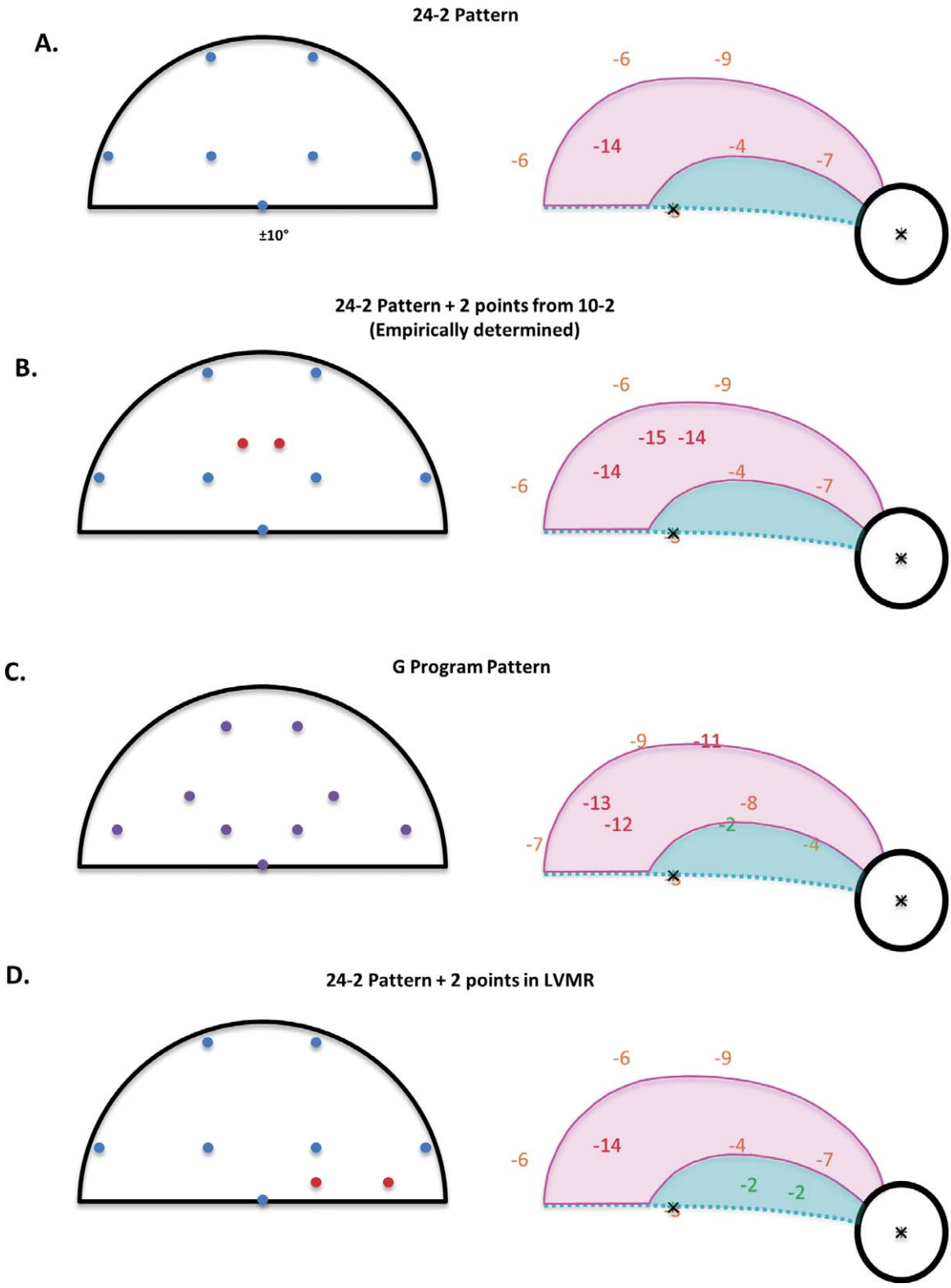

Figure 6. The simulated results for four visual field test patterns. The *left panels* show the simulated test patterns. (A) The 24-2 locations (*blue*); (B) The 24-2 points (*blue*) with two points (*red*) added to maximize the number of points ≤ -5 dB. (C) The G program, which has the same number of points as in B, but different locations (*purple*). (D) The 24-2 points (*blue*) with two points (*red*) added in the LVMR. The right panels show the mean TD values for the 31 eyes from Figure 4A for the locations in the *left panel*.

Table 3. Results of Simulations of Alternative VF Test Patterns

Field Pattern	# of Points	Mean # of Points Abnormal (≤ -5 dB)	Mean Percent of Points Abnormal (≤ -5 dB)
24-2	7	3.06	43.7%
24-2 +2 from 10-2 (Empirical)	9	4.61	51.2%
G Program	9	3.94	43.8%
24-2 +2 in LVMR	9	3.19	35.4%

results. On average, 3.06 (i.e., 43.7%) of the seven points had a TD of less than or equal to −5 dB.

In Figure 6B, we added the two points (in red) to the 24-2 pattern in panel A. The locations of the points were chosen from the locations in a 10-2 test pattern based upon an empirical simulation. That is, of the possible two 10-2 locations we could add to the upper VF, these two, located at (−1°, 5°) and (1°, 5°), produced the greatest percent of points with TDs less than or equal to −5 dB. This resulted in an average 4.61 points less than or equal to −5 dB or 51.2% of the nine points, significantly higher ($P < 0.001$) than the 24-2 pattern. The G program in the Octopus machine also has nine points within the central 10° of the upper VF as shown in Figure 6C. This pattern does better than the 24-2 (Fig. 6A, $P < 0.01$), but not quite as well as the modified 24-2 in Figure 6B, on average 3.94 versus 4.61 points less than or equal to −5 dB ($P = 0.01$). Finally, as a control for the number of points, we simulated a pattern in which two points were added inside the LVMR. As expected, this pattern did not do as well as the pattern with the two points within the VMR.

Discussion

Glaucomatous damage of the macula is more common in the upper VF, where local and deep arcuate defects can appear near fixation.[13,15,16,18] The typically employed VF test pattern, the 24-2, can underestimate and even miss these arcuate, upper VF defects.[5,13,18] The anatomical basis for this is now clear. The local RGC layer thinning associated with these upper VF defects falls largely within the central-most four points of the 24-2 test.[2,3] For these reasons, we focused on the upper VF in this study.

Both versions of a model of upper VF damage described the results of high-density perimetry. Interestingly, the standard version, in which the same model was applied to the data of all eyes, on average did as well as the aligned version, which was scaled and rotated based upon the individual's fovea-to-disc axis. There was a suggestion, however, that the aligned model might fit better for extreme anatomical differences (Table 2). This is consistent with previous work showing decreased anatomical variation in retinal nerve fiber patterns among healthy controls after fovea-to-disc alignment,[5,23–25] as well as improved mapping of VF locations to optic disc regions.[26,27] In any case, it appears that relatively little will be gained by taking differences in individual anatomy into consideration when deciding where to add test points to the 24-2 pattern. Future studies should assess whether the marginal benefits justify the additional procedure.

In any case, the similarity of the results for the standard and aligned model allows us to use the standard model to explore the consequences of adding points to the 24-2 pattern. In our simulations, we added only two points and restricted these points to the 10-2 test locations in our high-density grid. Based upon simulations, the optimal locations of these points were in the VMR, as predicted by the model (Fig. 6B). As an alternative to the 24-2 pattern for detecting glaucoma, the G-program was designed to improve detection of glaucomatous damage. For this pattern, two points were added in the macular region and the remaining seven points of the 24-2 pattern were rearranged to take anatomy into consideration. We found that the G program (Fig. 6C) did better than the 24-2 (Fig. 6A). However, the pattern in Figure 6B, in which two points were added to the 24-2 in the VMR, performed even better. As a control, we added two points to the LVMR (Fig. 6D). This added relatively little to detectability, as expected, despite having more points in the macular region than the 24-2 pattern.

Limitations and Future Directions

The questions left unanswered by this study illustrate its limitations and suggest future research projects. First, how many points should be added to the 24-2 test pattern and where should they be placed? The answer to this question will depend upon the value placed on different factors. We[5] have previously suggested performing a 10-2 VF test if there is any

suggestion of macular damage including: one or more of the central four points appear abnormal, visual acuity is poor, or the patient's complaints are consistent with macular damage. Adding all the points in a 10-2 (2° grid) pattern to the 24-2 (6° grid) pattern might be ideal if time were not a factor. However, time is a factor in the clinic, and patient fatigue is as well. Thus, it makes sense to add a few points to the center of the 24-2 pattern to increase its sensitivity/specificity for detecting macular damage. The two points added in our simulations (Fig. 6B) have the advantage of being included in the 10-2 test pattern so that if a 10-2 is subsequently performed these points are replicated. In any case, a prospective study of patients with early damage is needed to compare the sensitivity/specificity of this modified pattern with that of alternative approaches of detecting macular damage. One approach is to revise the entire test pattern to optimize detection of glaucomatous damage both within and outside the macula, while a second is to tailor the pattern based upon an individual's defect as seen on fundus photographs[17] or OCT scans.

Second, what about macular damage to the lower VF? Macular damage of the lower VF is typically less common, less severe, and usually further from fixation[9,13,15,16,18] as also predicted by the model.[17] Because this damage tends to be at the edge of the macula, it is more likely to be detected by the 24-2 test. However, this too needs to be confirmed in a prospective study. This prospective study should also contain a larger sample to overcome another limitation of the present study, its relatively small sample of 31 eyes.

The prospective study should also consider whether the enhanced 24-2 pattern will detect the milder, widespread damage that also occurs in the macula.[6,28–31] Because this damage tends to extend outside the macula, it too will likely be detected on a 24-2 test, especially with the additional points.

In any case, it is time to modify or replace the 24-2 test pattern to better detect macular damage due to glaucoma. If the goal is to compare new VF data with previous data, it is easiest to add a few points. As a minimum we suggest adding the two points identified in this study.

Acknowledgments

The authors thank those involved in the recruiting and testing of the patients in this study, including Danilo B. Fernandes, Bogomil Voykov, Andrea Mast, Regine Grund, Christine Talamini, and Ilana Traynis.

Supported by National Institutes of Health Grant R01-EY-02115 (DCH), and an equipment grant from Haag-Streit, Inc.

Disclosure: **D.C. Hood**, Topcon, Inc. (F); **M. Nguyen,** None; **A.C. Ehrlich,** None; **A.S. Raza**, None; **C.G. De Moraes**, None; **I. Sliesoraityte**, None; **R. Ritch**, None; **U. Schiefer**, Haag-Streit, Inc. (C, P)

References

1. Curcio CA, Allen KA. Topography of ganglion cells in human retina. *J Comp Neurol*. 1990;300:5–25.
2. Nelson P, Aspinall P, Papasouliotis O, Worton B, O'Brien C. Quality of life in glaucoma and its relationship with visual function. *J Glaucoma*. 2003;12:139–150.
3. Richman J, Lorenzana LL, Lankaranian D, et al. Importance of visual acuity and contrast sensitivity in patients with glaucoma. *Arch Ophthalmol*. 2010;128:1576–1582.
4. Hood DC, Raza AS, de Moraes CG, Johnson CA, Liebmann JM, Ritch R. The nature of macular damage in glaucoma as revealed by averaging optical coherence tomography data. *Transl Vis Sci Technol*. 2012;1:1–15.
5. Hood DC, Raza AS, de Moraes CG, Liebmann JM, Ritch R. Glaucomatous damage of the macula. *Prog Retin Eye Res*. 2013;32:1–21.
6. Hood DC, Slobodnick A, Raza AS, de Moraes CG, Teng CC, Ritch R. Early glaucoma involves both deep local, and shallow widespread, retinal nerve fiber damage of the macular region. *Invest Ophthalmol Vis Sci*. 2014;55:632–649.
7. Aulhorn E, Harms M. Early visual field defects in glaucoma. In: Leydhecker W, ed. *Glaucoma, Tutzing Symposium*. Basel, Switzerland: Karger; 1967:151–186.
8. Drance SM. The early field defects in glaucoma. *Invest Ophthalmol*. 1969;8:84–91.
9. Aulhorn E, Karmeyer H. Frequency distribution in early glaucomatous visual field defects. *Doc Ophthalmol Proc Ser*. 1977;14:75–83.
10. Anctil JL, Anderson DR. Early foveal involvement and generalized depression of the visual

field in glaucoma. *Arch Ophthalmol*. 1984;102: 363–370.
11. Heijl A, Lundqvist L. The frequency distribution of earliest glaucomatous visual field defects documented by automatic perimetry. *Acta Ophthalmol (Copenh)*. 1984;62:658–664.
12. Langerhorst CT, Carenini LL, Bakker D, De Bie-Raakman MAC. Measurements for description of very early glaucomatous field defects. In: Wall M, Heijl A, eds. Perimetry Update 1996/1997. *New York, NY: Kugler Publications;* 1997:67–73.
13. Schiefer U, Papageorgiou E, Sample PA, et al. Spatial pattern of glaucomatous visual field loss obtained with regionally condensed stimulus arrangements. *Invest Ophthalmol Vis Sci*. 2010; 51:5685–5689.
14. Park SC, De Moraes CG, Teng CC, Tello C, Liebmann JM, Ritch R. Initial parafoveal versus peripheral scotomas in glaucoma: risk factors and visual field characteristics. *Ophthalmology*. 2011; 118:1782–1789.
15. Su D, Park SC, Simonson JL, Liebmann JM, Ritch R. Progression pattern of initial parafoveal scotomas in glaucoma. *Ophthalmology*. 2013;120: 520–527.
16. Traynis I, de Moraes CG, Raza AS, Liebmann JM, Ritch R, Hood DC. The prevalence and nature of early glaucomatous defects in the central 10° of the visual field. *JAMA Ophthalmol*. 2014;132:291–297.
17. Schiefer U, Flad M, Stumpp F, et al. Increased detection rate of glaucomatous visual field damage with locally condensed grids: a comparison between fundus-oriented perimetry and conventional visual field examination. *Arch Ophthalmol*. 2003;121:458–465.
18. Hood DC, Raza AS, de Moraes CG, et al. Initial arcuate defects within the central 10 degrees in glaucoma. *Invest Ophthalmol Vis Sci*. 2011;52: 940–946.
19. Schiefer U, Pascual JP, Edmunds B, et al. Comparison of the new perimetric "German Adaptive Threshold Estimation" (GATE) strategy with conventional full-threshold and SITA Standard strategies. *Invest Ophthalmol Vis Sci*. 2009;50:488–494.
20. Drasdo N, Millican CL, Katholi CR, Curcio CA. The length of the Henle fibers in the human retina and a model of ganglion receptive field density in the visual field. *Vision Res*. 2007;47:2901–2911.
21. Raza AS, Cho JS, de Moraes CGV, et al. Retinal ganglion cell layer thickness and local visual field sensitivity in glaucoma. *Arch Ophthalmol*. 2011; 129:1529–1536.
22. Hood DC, Raza AS. Method for comparing visual field defects to local RNFL and RGC damage seen on frequency domain OCT in patients with glaucoma. *Biomed Opt Express*. 2011;2:1097–1105.
23. Jansonius NM, Nevalainen J, Selig B, et al. A mathematical description of nerve fiber bundle trajectories and their variability in the human retina. *Vision Res*. 2009;49:2157–2163.
24. Jansonius NM, Schiefer J, Nevalainen J, Paetzold J, Schiefer U. A mathematical model for describing the retinal nerve fiber bundle trajectories in the human eye: average course, variability, and influence of refraction, optic disc size and optic disc position. *Exp Eye Res*. 2012;105:70–78.
25. Denniss J, Turpin A, Tanabe F, Matsumoto C, McKendrick AM. Structure-function mapping: variability and conviction in tracing retinal nerve fiber bundles and comparison to a computational model. *Invest Ophthalmol Vis Sci*. 2014;55:728–736.
26. Denniss J, McKendrick AM, Turpin A. An anatomically customizable computational model relating the visual field to the optic nerve head in individual eyes. *Invest Ophthalmol Vis Sci*. 2012; 53:6981–6990.
27. Denniss J, Turpin A, McKendrick AM. Individualized structure-function mapping for glaucoma: practical constraints on map resolution for clinical and research applications. *Invest Ophthalmol Vis Sci*. 2014;55:1985–1993.
28. Henson DB, Artes PH, Chauhan BC. Diffuse loss of sensitivity in early glaucoma. *Invest Ophthalmol Vis Sci*. 1999;40:3147–3151.
29. Drance SM. Diffuse visual field loss in open-angle glaucoma. *Ophthalmology*. 1991;98:1533–1538.
30. Caprioli J, Sears M, Miller JM. Patterns of early visual field loss in open-angle glaucoma. *Am J Ophthalmol*. 1987;103:521–517.
31. Artes PH, Chauhan BC, Keltner JL, et al; for the Ocular Hypertension Treatment Study Group. Longitudinal and cross-sectional analyses of visual field progression in participants of the Ocular Hypertension Treatment Study. *Arch Ophthalmol*. 2010;128:1528–3152.